Engineering Structures 131 (2017) 57–68

Contents lists available at ScienceDirect

Engineering Structures

journal homepage: www.elsevier.com/locate/engstruct

A two-dimensional IB-LBM framework combined with re-tailored RCVM for assessing the rotation intensity of a tornadic wind over a building configuration

Xixiong Guo, Rangaraj Palanisamy, Jun Cao *

Department of Mechanical and Industrial Engineering, Ryerson University, Toronto, Ontario M5B 2K3, Canada

ARTICLE INFO

Article history:
Received 11 July 2016
Revised 5 October 2016
Accepted 13 October 2016
Available online 2 November 2016

Keywords:
Tornadic wind
Rankine-combined vortex model
Immersed boundary lattice Boltzmann method (IB-LBM)
Rotation intensity
Building configuration

ABSTRACT

A tornado is fundamentally a devastating airflow featuring simultaneous translation and rotation. This hybrid nature makes the simulations more interesting as well as challenging. Numerous laboratorial and computational simulations of tornadoes have been performed in the past few decades to study the tornado dynamics. This study concentrates on the tornado-structure interaction through numerical simulation. Establishing a set of physically-rational and meanwhile computationally-maneuverable boundary conditions for the tornado-building interaction scenario poses a challenge to numerical simulation developers. Inspired by the recent progress in the application of immersed-boundary (IB) lattice Boltzmann method (LBM) to the fluid-structure interaction simulations, this study presents an IB-LBM framework and, meanwhile, revises the renowned Rankine-Combined Vortex Model (RCVM) with the aid of the "relative motion" principle, such that the challenging boundary condition setup issue can be successfully resolved. The present IB-LBM simulations are aimed to investigate the tornado-like wind effects on a building configuration in different orientations and, particularly, seek the relation between the rotation intensity of a tornado and the tornadic wind loadings on the constructions. Through examinations at a series of rotation intensities, the extreme loading value is observed to be unrelated to Reynolds number once the rotation intensity exceeds a critical value. These simulation results reveal that it looks inappropriate to rely solely on the translational velocity component to characterize tornadoes, and call on additional attention towards the rotation intensity for a more comprehensive tornado dynamics study.

1. Introduction

Tornadoes are natural catastrophes that may cause unimaginable property damages and loss of lives every year. The combination of rotation and translation makes the tornadic wind more cataclysmic when compared to a straight-line wind. A structure, in spite of its proper design and quality construction against the wind of straight-line type, might collapse under a tornadic wind of the same translational speed due to the concurrent rotational feature of tornadic wind [1]. Therefore, it is crucial to understand the loadings induced by a tornadic wind onto buildings and the factors affecting the loadings.

Rotation intensity, defined as the ratio of the maximum tangential flow rate of the rotational component to the translational speed, is presented in this study as a quantitative factor that is strongly related to the tornadic wind loadings. In order to better prevent building destruction from tornadoes, a more thorough understanding of tornado-induced wind loads is required to enhance the wind-resistant capabilities of buildings. Furthermore, investigation into the influences of the rotational component of a tornado can also gain complementary insight for civil engineers in their building designs.

The tornado dynamics has been studied through both laboratorial experiments and numerical simulations. Ward [2] first developed a laboratorial tornado-simulator that could produce a stationary tornado-like wind but without any translation movement taken into account. Then alterations [3–5] have been made by other researchers to construct a more convincing simulator. However, investigation through laboratory experiments tends to be time-consuming, restrictive, and expensive. With the advancement in computer technology, numerical studies have been introduced for tornado-like wind simulations over the past few decades. Wilson and Rotunno [6] first applied a two-dimensional numerical

* Corresponding author.
E-mail address: jcao@ryerson.ca (J. Cao).

http://dx.doi.org/10.1016/j.engstruct.2016.10.016
0141-0296/

model to study the tornado-structure interactions on rectangular-shaped buildings. Nolan and Farrell [7] utilized the axisymmetric Navier-Stokes (N-S) equations with a constant viscosity to explore the structure and dynamics of tornado-like vortices. Lewellen et al. [8,9] used three-dimensional large eddy simulation (LES) turbulence model to investigate the dynamics of a tornado-like vortex near the surface. Ishihara et al. [10] developed a numerical simulation model by incorporating LES in the time-dependent N-S equations to look into the flow fields of one-celled and two-celled vortices. In addition to the reported investigations on the vortex core, the tornado-induced wind loadings and tornado-structure interaction are separate significant topics that have also received specific attention. Bienkiewicz and Dudhia [11] conducted comparative studies to measure wind loads and surface pressure on small building models in swirling, tornado-like winds and straight-line winds. The results revealed that the wind loads on the tested models are significantly higher (3–5 times) in swirling and tornado-like winds than in the straight-line winds, and surface pressure distributions on the tested building models are also quite different compared to those in straight-line winds. These observations further proved that the tornado-like wind with a drastic rotation can generate much higher loadings than a straight line wind. The numerical simulations conducted by Selvam et al. [12–14] placed their focus on the tornado-building interaction, which is of more practical significance. They reported the tornado-induced loads on 2D sections of a cylinder and multi-cubic buildings using the finite difference discretization of the N-S equations [12,13], and also extended their simulations to 3D cases [14] together with the case of tornadoes at elevated Reynolds numbers with the aid of a LES model [15]; otherwise, numerical simulation work is rarely seen that concentrates on the tornadic wind loads exerted on building structures.

It is noticed that the reported computational analysis of tornado dynamics has placed more emphasis on the translational component since the translational velocity is conventionally chosen to serve as the characteristic velocity for the Reynolds number definition. Physically, both the translational and rotational components co-exist in a tornado wind field. The evaluation of the overall tornado wind loading without due consideration of the influence of the rotational component would turn out to be inaccurate and unreliable, possibly leading a structural design to miscalculated wind-resistant capabilities; however, the relation between the overall tornado wind load and its rotational component has been seldom reported in existing literature. In order to gain a better understanding in this regard, this study aims to scrutinize the correlation between the aerodynamic loads and the rotational component of a tornadic wind by means of numerical simulation.

Commonly, the aforementioned computer simulations [8–13] were all based on the N-S solver via classical numerical approaches. The highly dynamic nature of the tornado-like wind necessitates the boundary conditions of the flow field to be updated every time step, and it becomes tedious in the traditional method. Breakthrough is demanded to deal with such a simultaneously translating and rotating airflow by introducing emerging and yet promising numerical schemes. However, very little work has been found in seeking novel numerical tools to address this topic.

As an alternative to the N-S equations based solver, the lattice Boltzmann method (LBM) [16] has been established as an effective numerical scheme for simulating viscous flow in recent years due to its noticeable advantages in terms of simplicity for implementation, parallelizability for algorithmic development, and robustness for applications [16–18]. On the other hand, the immersed boundary (IB) method proposed by Peskin [19,20]is a widespread approach dealing with moving boundary problem. As a non-boundary conforming method, IB introduces an additional "restoring" force in the vicinity of a moving object that is immersed in a fluid, so that all the effects of the fluid to the boundary of the solid object can be accounted for and, then, by using a discrete Delta function, this additional force is distributed back as a special body force at the affected grid nodes. In 2004, the IB scheme was successfully incorporated in LBM by Feng and Michaelides [21]. They demonstrated some remarkable advantages of IB-LBM when simulating two-dimensional and three-dimensional particulate flow [22]. Then, IB-LBM has been extensively utilized in solving challenging fluid-solid interaction (FSI) problems in a number of scenarios including flapping/flexible foil [23,24], flapping of multiple elastic structures [25], particulate-fluid interaction [26], and solid-liquid phase change [27].

Inspired by the reported IB-LBM application success [21–27], this study intends to open a novel IB-LBM outlet for the tornado-building interaction simulation. As the tornado-like wind can be decomposed, according to the Rankine-combined vortex model (RCVM), into two components, namely rotation and translation, the scenario of a tornado towards a building is interpreted, in this study, by a "virtual" translation of the building towards a "purely" rotating airflow about its "locked" center, which implies the application of the "relative motion" principle only to the translation component of the tornado; then, the IB approach is employed to mathematically model the "moving" building. This innovative interpretation of the tornado-building interaction greatly facilitates the establishment of boundary conditions, such that the outer boundary of the tornado-like wind domain can be prescribed by simply using the time-independent rotation part of the tornado, as extracted from RCVM, while the satisfaction of the "no-slip" boundary condition for the building is guaranteed by the IB approach. Guided by this new interpretation, this study aims at the simulation of tornado-like winds at different rotation intensities over a building configuration with orientation deployed, while the focus is placed on a parametric study for each of the tested orientations towards capturing a critical rotation intensity that discontinues the monotonically increasing relation between the tornadic wind loading and Reynolds number.

The rest of this paper will unfold as follows. Section 2 describes the RCVM for tornado-like flow and presents its customization. Section 3 outlines the IB-LBM framework for this study, followed by a case study for validation purpose, as demonstrated in Section 4. In Section 5, a series of detailed simulation results are demonstrated to elucidate the overall effects of rotational components onto a stylized configuration in different orientations. Finally, remarks are made in Section 6, addressing the conclusion and possible extension of this study.

2. Tornado-like flow model

2.1. Rankine-combined vortex model (RCVM)

The Rankine-combined vortex model (RCVM) is the simplest model to describe a tornado flow domain. RCVM has a distinct advantage of satisfying the Navier-Stokes equation[12] in both the free-vortex and forced-vortex regions of the tornado flow domain. But its limitation is that it can be applied only to a two-dimensional obstacle-free domain. In RCVM, the tornado velocity profile can be decomposed into a constant-translation component, $\vec{V}_t$, and a component of rotation with respect to the wind center, $\vec{V}_\theta$, which denotes the tangential velocity component. Let r and r_c respectively represent the radius from the tornado center and the maximum radius of the forced-vortex region (also the location of the maximum tangential velocity). When r is less than r_c, V_θ varies linearly with r. At radii larger than r_c, i.e., in the free-vortex region,

V_θ decreases with the radius. The overall mathematical expression of RCVM is:

$$V_\theta = \begin{cases} r\omega, & r \leqslant r_c \\ r_c^2\omega/r, & r > r_c \end{cases} \tag{1}$$

where ω is the constant angular velocity.

As aforementioned, the conventional RCVM cannot be applied to the flow domain where a wind-obstacle interaction is present. Nevertheless, RCVM can serve to initialize the flow domain, physically representing the onset of a tornadic wind with its center separated from an obstacle by such a large margin that the mutual interaction at the very beginning can be considered fairly insignificant. Remark that the real tornado situation begins with a constant translational velocity, $\vec{V}_t = V_{tx}\vec{i} + V_{ty}\vec{j}$, which applies to the whole flow domain while the building remains immobile, in addition to the rotation about the moving wind center. In the light of RCVM, at a given time instant, t, the resultant velocity at a point (x, y) located in the counter-clockwise tornado rotation field reads:

$$\vec{V} = \vec{V}_t + \vec{V}_\theta = (V_{tx} - V_\theta \sin\theta)\,\vec{i} + (V_{ty} + V_\theta \cos\theta)\,\vec{j} \tag{2}$$

with

$$\theta = \tan^{-1}\left(\frac{y - y_c(t)}{x - x_c(t)}\right) \tag{3}$$

where $x_c(t) = x_{c0} + v_{tx}t$ and $y_c(t) = y_{c0} + v_{ty}t$, and θ represents the angle between the radial line passing through (x, y) and the horizontal direction pointing to the right. Obviously, $\vec{V} = \vec{V}(x, y, t)$ because of $\theta = \theta(x, y, t)$.

2.2. Custom-made RCVM

The analysis of the resultant velocity in RCVM reveals its time-dependent nature. If RCVM is employed to stipulate the boundary conditions, then updating the boundary conditions becomes mandatory, which presents high computational complexity if purely relying on conventional Computational Fluid Dynamics (CFD) methods without any other pertinent numerical treatment.

This tornado study is intended to modify the classical RCVM in such a way that the boundary conditions are still established on the basis of RCVM but in a time-independent form. This task can be accomplished by using the concept of "relative motion". This concept allows for detaching the translation velocity component from RCVM and re-attaching this component to the obstructed building, as if the tornado center gets "*riveted*", i.e., $x_c(t) \equiv x_{c0}$, $y_c(t) \equiv y_{c0}$, while the building is viewed as "*in motion*" with a velocity that is equal to the original translation magnitude but opposite to the real tornado translation direction. Consequently, the vortex-structure interaction scenario can be described as the building "*virtually entering*", at a translational velocity $\vec{V}_t = -(V_{tx}\vec{i} + V_{ty}\vec{j})$, a "*purely*" rotational airflow $\vec{V}_\theta = V_\theta(-\vec{i}\sin\theta + \vec{j}\cos\theta)$ in which $\theta = \tan^{-1}\left(\frac{y-y_{c0}}{x-x_{c0}}\right)$ becomes no longer related to the time, t. As illustrated in Fig. 1, this new representation eases setting up the boundary condition such that the velocity at the outer boundary of the simulation domain includes only the rotational component, which requires no updating with the elapsing time. The "*virtual translation*" of the building can be modeled by the immersed boundary (IB) approach, which will be described in Section 3.2. The boundary conditions afforded by this re-tailored RCVM appear both physically compatible with the flow nature and numerically much more maneuverable.

2.3. Rotation intensity in tornadic wind

This study is mainly focused on the investigation of the impact of intensity of the rotation component in a tornadic flow, which is denoted by β:

$$(V_\theta)_{\max} = r_c\omega = \beta V_t \tag{4}$$

where β represents the ratio of $(V_\theta)_{\max}$, the maximum tangential flow rate of the rotational component, to V_t, the translational flow rate. The larger the value of β, the more dominant the rotation component in the tornadic flow. Detailed numerical experiments will be presented in Section 5, addressing the influence of the rotation intensity on the aerodynamic loadings.

3. Numerical method

3.1. Lattice Boltzmann model with multiple-relaxation-time collision

In describing incompressible fluid flows, the lattice Boltzmann model (LBM) [28] interprets each time step with two processes, namely streaming and collision. In the streaming process, each fluid particle moves to the nearest node, whereas in the collision process the particles coming to a node collide and change their velocity directions. In this model, the flow domain is discretized into uniform square lattices with unit spacing. Among available numerical lattice schemes, the simple and popular D2Q9 model is selected for this tornado study. In the D2Q9 model, there are totally 9 nodes, and a particle residing at a node can travel to any one of the nearest 8 neighbor nodes at each time step along a connecting link. The lattice speed is defined by $c = \delta x/\delta t$, equal to 1, where δx is the lattice size, and δt the time step. The particles are categorized into three types based on their speeds and moving directions: particles of type 1 have zero speed and stay at the same node, particles of type 2 move along the axes at a speed of c, whereas particles of type 3 move in the diagonal directions with a speed of $\sqrt{2}c$. The particle velocity set in D2Q9 can be summarized as follows:

$$c_i = \begin{cases} (0,0) & i = 0 \\ (\cos[(i-1)\pi/2], \sin[(i-1)\pi/2])c, & i = 1,2,3,4 \\ (\cos[(2i-9)\pi/4], \sin[(2i-9)\pi/4])\sqrt{2}c, & i = 5,6,7,8 \end{cases} \tag{5}$$

Based upon the lattice Boltzmann equation (LBE), the governing equation for multiple-relaxation-time (MRT) – LBM takes the following form:

$$\boldsymbol{f}(\boldsymbol{x} + \boldsymbol{c}_i\delta_t, t + \delta_t) - \boldsymbol{f}(\boldsymbol{x}, t) = -\mathbf{M}^{-1}\mathbf{S}[\boldsymbol{R}(\boldsymbol{x}, t) - \boldsymbol{R}^{eq}(\boldsymbol{x}, t)] \tag{6}$$

where $\boldsymbol{f}$ is the vector composed of distribution functions, $\mathbf{M}$ is the transformation matrix, $\mathbf{S}$ is the diagonal relaxation matrix, $\boldsymbol{R}$ is the moment vector, $\boldsymbol{R}^{eq}$ is the corresponding equilibrium moment vector. The detailed forms of these vectors and matrices are given below:

$$\boldsymbol{f} = (f_0, f_1, f_2, f_3, f_4, f_5, f_6, f_7, f_8)^T \tag{7}$$

$$\mathbf{S} = diag(s_0, s_1, \ldots, s_8) = diag(0, s_e, s_\varepsilon, 0, s_q, 0, s_q, s_v, s_v) \tag{8}$$

$$\boldsymbol{R} = (\rho, e, \varepsilon, j_x, q_x, j_y, q_y, p_{xx}, p_{xy})^T \tag{9}$$

$$\boldsymbol{R}^{eq} = \rho(1, -2 + 3u^2, 1 - 3u^2, u_x, -u_x, u_y, -u_y, u_x^2 - u_y^2, u_x u_y)^T \tag{10}$$

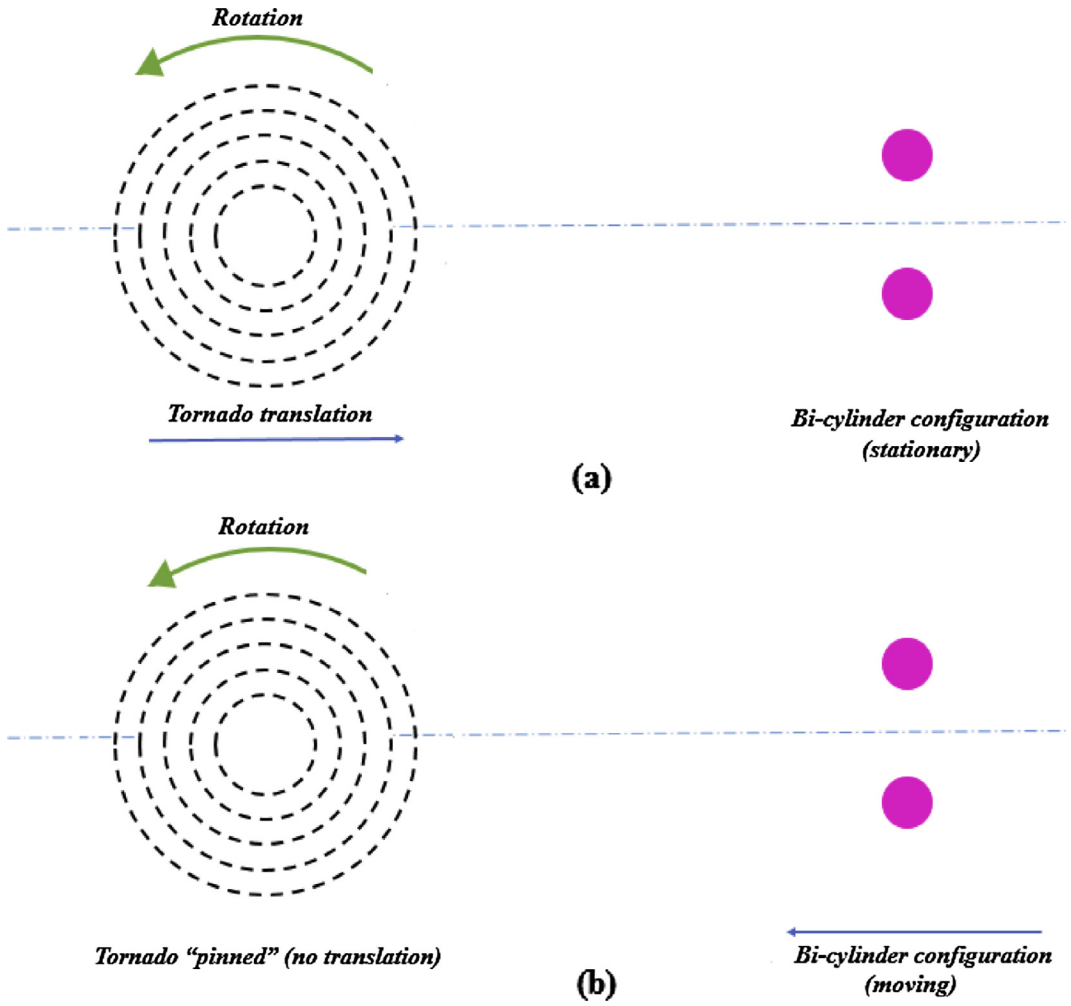

Fig. 1. Physical and re-tailored RCVM's (a) Physical tornado kinematics; (b) Re-tailored tornado model.

$$\mathbf{M} = \begin{pmatrix} 1 & 1 & 1 & 1 & 1 & 1 & 1 & 1 & 1 \\ -4 & -1 & -1 & -1 & -1 & 2 & 2 & 2 & 2 \\ 4 & -2 & -2 & -2 & -2 & 1 & 1 & 1 & 1 \\ 0 & 1 & 0 & -1 & 0 & 1 & -1 & -1 & 1 \\ 0 & -2 & 0 & 2 & 0 & 1 & -1 & -1 & 1 \\ 0 & 0 & 1 & 0 & -1 & 1 & 1 & -1 & -1 \\ 0 & 0 & -2 & 0 & 2 & 1 & 1 & -1 & -1 \\ 0 & 1 & -1 & 1 & -1 & 0 & 0 & 0 & 0 \\ 0 & 0 & 0 & 0 & 0 & 1 & -1 & 1 & -1 \end{pmatrix} \tag{11}$$

Note that, in the relaxation matrix, $\mathbf{S}$, $s_0 = s_3 = s_5 = 0$ are acceptable, and recommended for reducing the cost of computation. The relaxation rates s_v and s_e are related to the kinematic and bulk viscosities, v and ζ, using:

$$v = c_s^2\left(\frac{1}{s_v} - \frac{1}{2}\right)\delta_t, \tag{12}$$

$$\zeta = c_s^2\left(\frac{1}{s_e} - \frac{1}{2}\right)\delta_t, \tag{13}$$

The relaxation rates s_e, s_q, s_ε can be adjusted within the interval of $(0, 2)$. The matrix $\mathbf{M}$ is applied to transform the distribution function $\boldsymbol{f}$ onto the moment space $\boldsymbol{R}$ such that $\boldsymbol{R} = \boldsymbol{Mf}$ and $\boldsymbol{R}^{eq} = \boldsymbol{Mf}^{eq}$. The components of the corresponding equilibrium distribution function, $\boldsymbol{f}^{eq}$, are given by:

$$f_i^{eq} = w_i\rho\left[1 + \frac{\boldsymbol{c}_i \cdot \boldsymbol{u}}{c_s^2} + \frac{(\boldsymbol{c}_i \cdot \boldsymbol{u})^2}{2c_s^4} - \frac{u^2}{2c_s^2}\right], \quad i = 0, 1, \ldots, 8 \tag{14}$$

where the coefficients are $w_0 = 4/9, w_1 = w_2 = w_3 = w_4 = 1/9$, $w_5 = w_6 = w_7 = w_8 = 1/36$, and the speed of sound takes $c_s = c/\sqrt{3}$.

The density, velocity of the fluid, and the pressure of the flow are determined as follows:

$$\rho = \sum_{i=0}^{8} f_i, \quad \boldsymbol{u} = \frac{1}{\rho}\sum_{i=0}^{8} f_i c_i, \quad p = \rho c_s^2 \tag{15}$$

3.2. Incorporation of immersed boundary (IB) approach in LBM

When applying the immersed boundary (IB) approach to a fluid flow problem, the effects of the interaction between the fluid and an immersed solid object are considered by an additional force term, such that the computational domain becomes also inclusive of the region occupied by the solid object. While integrating the IB approach in LBM, the flow field Ω is represented by a set of Eulerian points, which are the fixed Cartesian grid nodes in the LBM framework; meanwhile, the boundary of the immersed object, denoted by Γ, is described by a set of Lagrangian points, $\boldsymbol{X}_B^l$, where the superscript l and subscript B represent the Lagrangian point and the boundary of the immersed object, respectively. Remark that

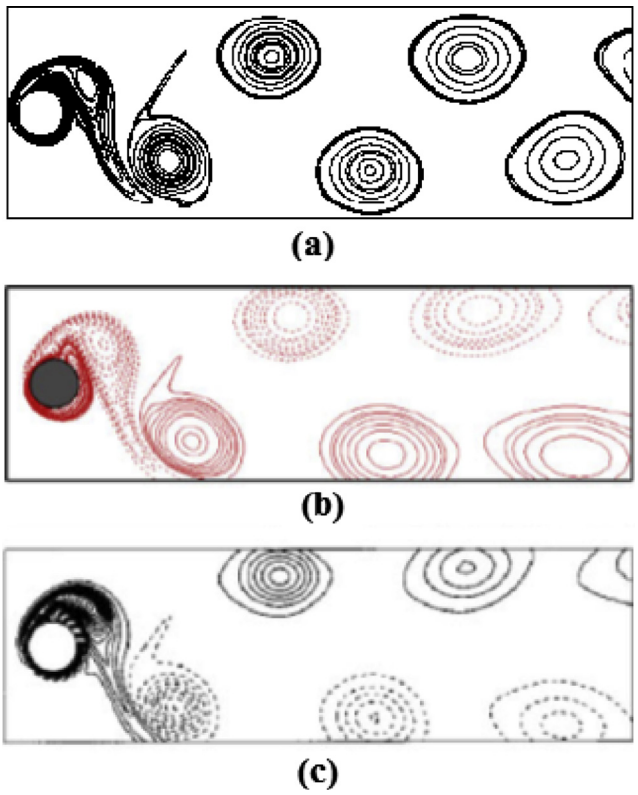

Fig. 2. Vorticity contour results from (a) the present method; (b) Wu et al. [32]; (c) Choi et al. [33].

Table 1
Comparison about the drag and lift coefficients at $Re = 100$.

References	Drag coefficient $\overline{C_d}$	Lift coefficient C_l'
Wu et al. [32]	1.302	0.321
Choi et al. [33]	1.231	0.299
Present	1.286	0.320

this series of points are referred to as Lagrangian points because the body itself, including its boundary, is not necessarily always at rest. An external force term reflecting the fluid-solid interaction, $\boldsymbol{f}_{RST}$, which is allocated at the Eulerian points within the neighborhood of the immersed boundary, should be numerically determined and then seamlessly added to the LBM framework. The IB and MRT-LBM incorporation is carried out through the following procedure:

Step 1: obtain the velocity $\boldsymbol{U}_B^l$ at the Lagrangian points $\boldsymbol{X}_B^l$

For measuring the closeness of an Eulerian point, $\boldsymbol{x}_{ij} = (x_i, y_j)^t$, and a Lagrangian point, $\boldsymbol{X}_B^l = \left(X_B^l, Y_B^l\right)^t$, the following continuous kernel distribution is required:

$$D_{ij}\left(\boldsymbol{x}_{ij} - \boldsymbol{X}_B^l\right) = \delta\left(x_i - X_B^l\right)\delta\left(y_j - Y_B^l\right) \tag{16}$$

where

$$\delta(r) = \begin{cases} \frac{1}{4}\left(1 + \cos\left(\frac{\pi|r|}{2}\right)\right), & |r| \leqslant 2 \\ 0, & |r| > 2 \end{cases} \tag{17}$$

which is proposed by Peskin [20]. While $\boldsymbol{u}(\boldsymbol{x}, t)$ is known at all Eulerian points, the velocity of the fluid particle adhered to a Lagrangian point $\boldsymbol{X}_B^l$ can be determined by:

$$\boldsymbol{U}_B^l(\boldsymbol{X}_B^l, t) = \boldsymbol{u}(\boldsymbol{X}_B^l, t) = \sum_{i,j} \boldsymbol{u}(\boldsymbol{x}, t) D_{ij}(\boldsymbol{x}_{ij} - \boldsymbol{X}_B^l)\delta x \delta y \tag{18}$$

with $\delta x = \delta y = 1$ in the present LBM framework. Note Eq. (18) indicates that the fluid velocity at a boundary point is equal to the solid boundary velocity at the same position, which ensures the "*no-slip*" condition at the boundary. Remark that a revised version of Eq. (17) can be found in [30], which might be of more help when the boundary of the immersed object contains singular points.

Step 2: Obtain the restoring force $\boldsymbol{F}_{RST}^l$ at Lagrangian points $\boldsymbol{X}_B^l$

After $\boldsymbol{U}_B^l$ is obtained at Lagrangian points, the restoring force per unit volume exerted at a Lagrangian point can be easily computed using the following feedback-forcing model [31]:

$$\boldsymbol{F}_{RST}^l = \alpha_1 \int_0^t \left(\boldsymbol{U}_B^l - \boldsymbol{U}_{IMS}\right) dt + \alpha_2 \left(\boldsymbol{U}_B^l - \boldsymbol{U}_{IMS}\right) \tag{19}$$

where α_1 and α_2 are two free negative constants with dimensions of $ML^{-3}T^{-2}$ and $ML^{-3}T^{-1}$, respectively. According to [31], α_1 and α_2 are stable for moderate values within $[-100, -1]$, and insensitive to their exact values. Also, note that $\boldsymbol{U}_{IMS}$ in Eq. (19) represents the velocity of the immersed body, which can be defined by:

$$\boldsymbol{U}_{IMS}(s, t) = \frac{\partial \boldsymbol{X}(s, t)}{\partial t} \tag{20}$$

and can be numerically determined using:

$$\boldsymbol{U}_{IMS}(s, t) = \frac{\boldsymbol{X}(s, t) - \boldsymbol{X}(s, t - \delta t)}{\delta t} \tag{21}$$

with s denoting the Lagrangian parametric coordinate. Note that $\boldsymbol{U}_{IMS} \equiv \boldsymbol{0}$ for a stationary immersed body, since $\boldsymbol{X} = \boldsymbol{X}(s)$ when the body does not move in the fluid.

Step 3: Obtain the restoring force $\boldsymbol{f}_{RST}$ at Eulerian points $\boldsymbol{x}_{ij}$

After $\boldsymbol{F}_{RST}^l$ is available at the Lagrangian points, the restoring force $\boldsymbol{f}_{RST}$ at Eulerian points, $\boldsymbol{x}_{ij}$, can be computed with the aid of continuous kernel distribution, as described in Eqs. (16) and (17). That is,

$$\boldsymbol{f}_{RST}(\boldsymbol{x}_{ij}, t) = \sum_l \boldsymbol{F}_{RST}^l\left(\boldsymbol{X}_B^l, t\right) D_{ij}\left(\boldsymbol{x}_{ij} - \boldsymbol{X}_B^l\right) \Delta s_l \tag{22}$$

where Δs_l is the arc length of the boundary segment.

Step 4: Embed the restoring force $\boldsymbol{f}_{RST}$ in LBM

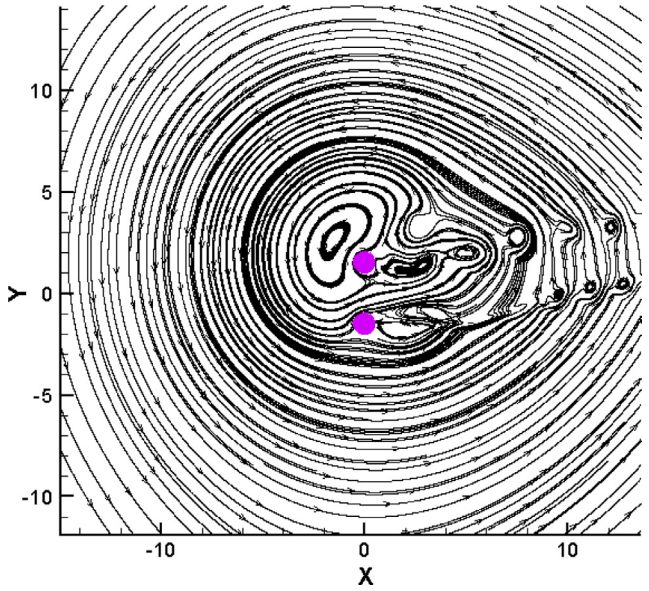

Fig. 3. Streamlines at "coinciding-center" time for vertically arranged bi-cylinders, at $Re = 1000$ and $\beta = 1.5$.

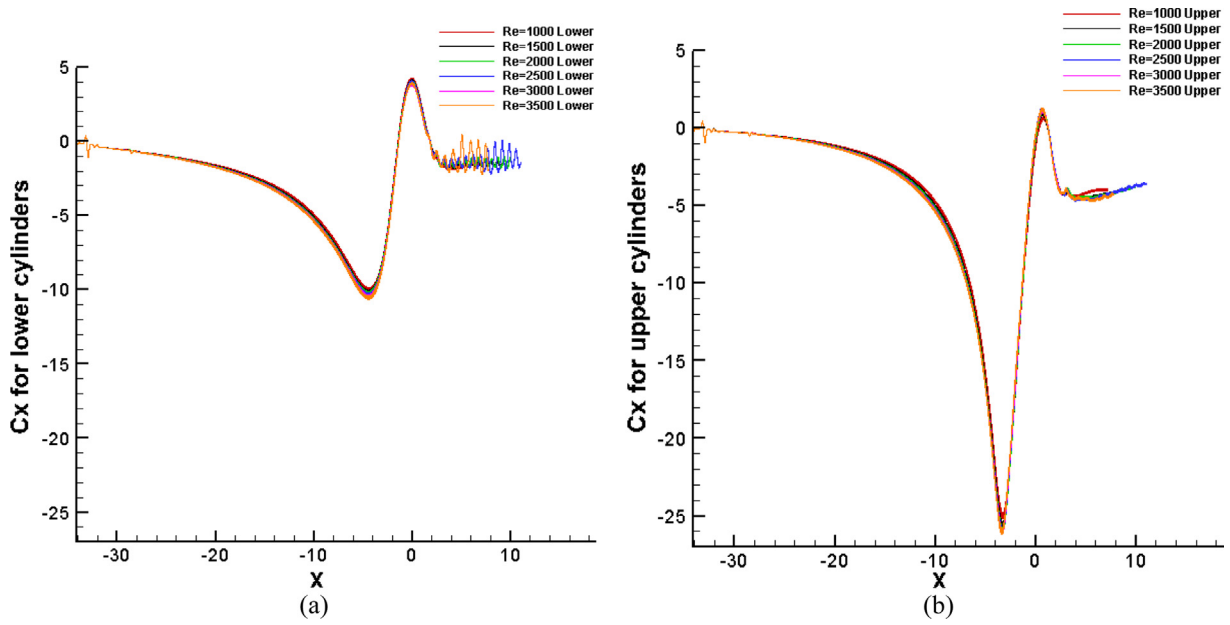

Fig. 4. C_x evolutions for vertically arranged bi-cylinders at $\beta = 1.5$, under different Re (a) lower cylinder; (b) upper cylinder.

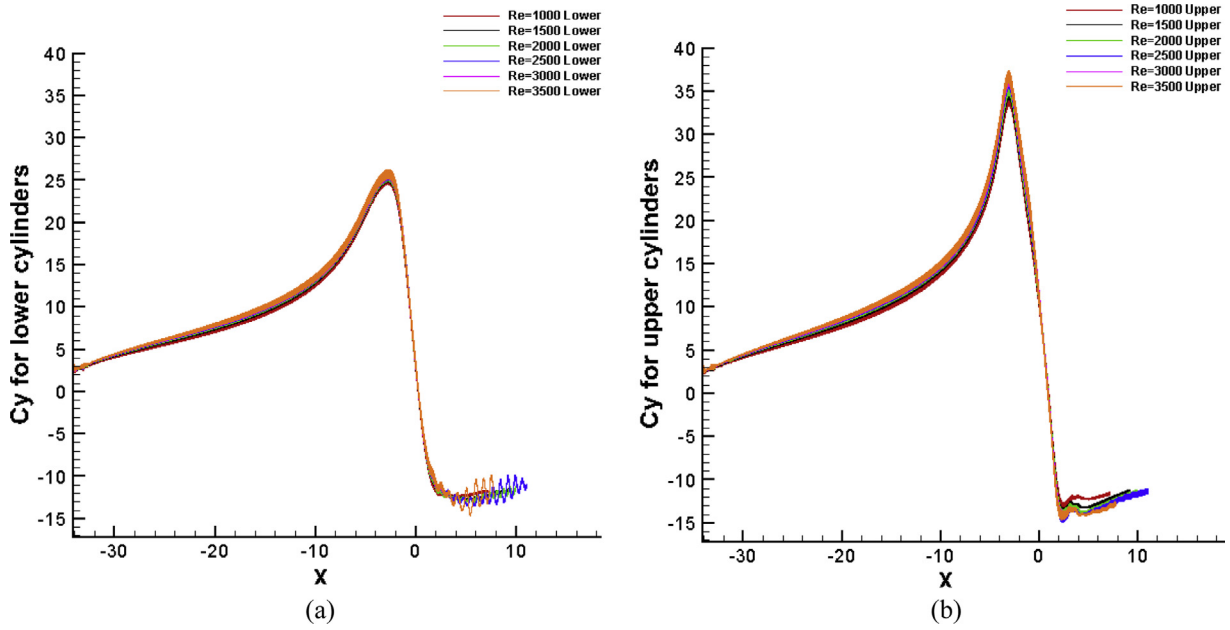

Fig. 5. C_y evolutions for vertically arranged bi-cylinders at $\beta = 1.5$, under different Re (a) lower cylinder; (b) upper cylinder.

In order to invoke $\boldsymbol{f}_{RST}$ in the LBM framework, the following transformation is employed:

$$\tilde{f}_i = \left(1 - \frac{1}{2\tau}\right) w_i \left(\frac{\boldsymbol{c}_i - \boldsymbol{u}}{c_s^2} + \frac{\boldsymbol{c}_i \cdot \boldsymbol{u}}{c_s^4}\boldsymbol{c}_i\right) \cdot \boldsymbol{f}_{RST} \tag{23}$$

where w_i represents the coefficients in the equilibrium distribution function mentioned in Eq. (14).

The inclusion of $\tilde{f}_i$ leads to the following revised LBE [29]:

$$f_i(\boldsymbol{x} + \boldsymbol{c}_i\delta t, t + \delta t) - f_i(\boldsymbol{x}, t) = -\frac{1}{\tau}\left(f_i(\boldsymbol{x}, t) - f_i^{eq}(\boldsymbol{x}, t)\right) + \tilde{f}_i\delta t \tag{24}$$

Finally, the velocity in the LBM framework has to be updated by including f_{RST} as follows:

$$\rho\boldsymbol{u} = \sum_{i=0}^{8} f_i\boldsymbol{c}_i + \frac{1}{2}\boldsymbol{f}_{RST}\delta t \tag{25}$$

4. Validation

As indicated in Section 1, very limited literature about numerical simulation of tornado-induced wind load on buildings can be found; in particular, those using RCVM as a model basis are even fewer. Thus, other comparable cases need to be sought to validate the present approach. The case of a flow induced by a counter-clockwisely rotationally oscillating cylinder, as numerically simulated in [32,33], is of some relevant interest to

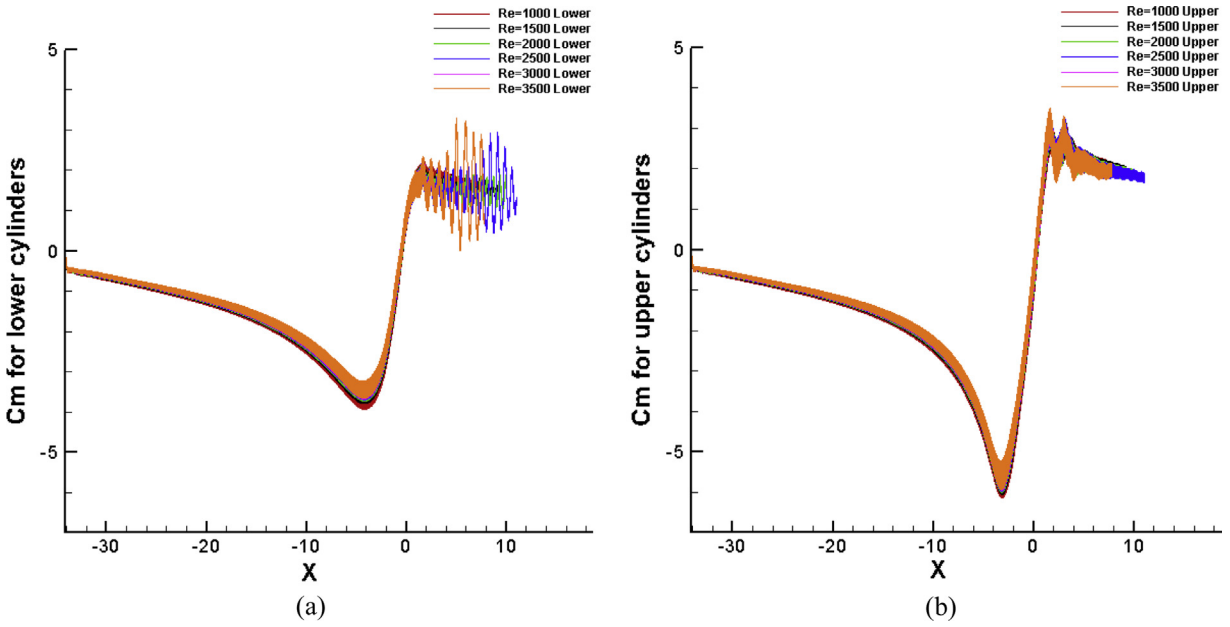

Fig. 6. C_m evolutions for vertically arranged bi-cylinders at $\beta = 1.5$, under different Re (a) lower cylinder; (b) upper cylinder.

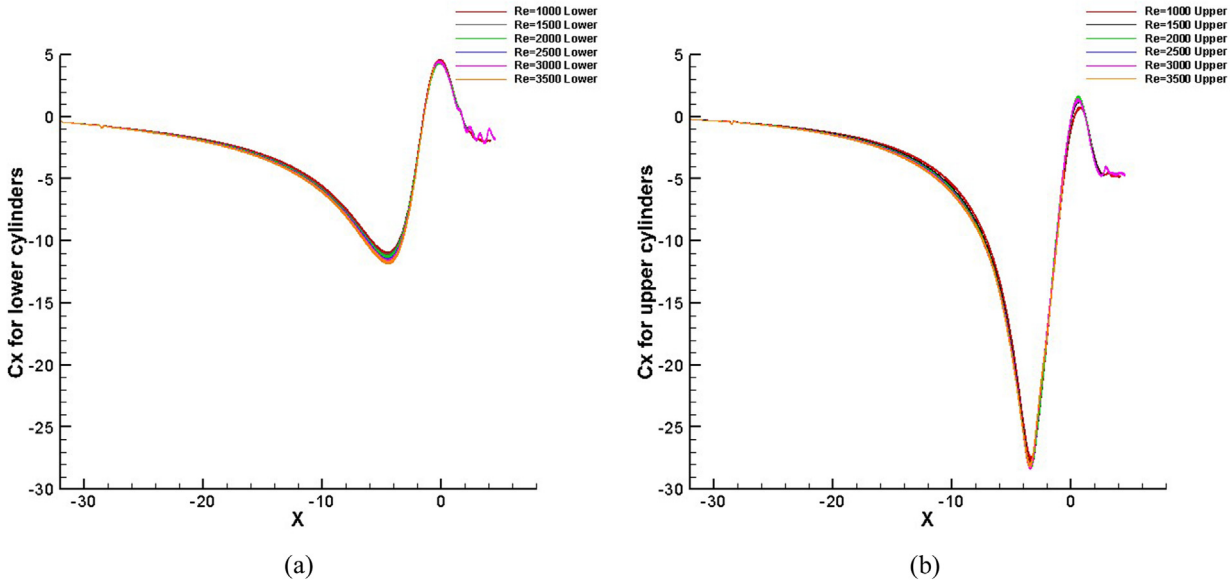

Fig. 7. C_x evolutions for vertically arranged bi-cylinders at $\beta = 2$, under different Re (a) lower cylinder; (b) upper cylinder.

tornado simulation, since that case also involves the fluid dynamics due to a fairly complex rotation. The rotationally oscillating cylinder induced flow simulation is hence chosen to test the present IB-LBM framework and, particularly, its applicability to the rotational flow evolution simulation.

All IB-LBM simulations performed in this study use a uniform grid ($\delta x = \delta y = 1$) based on the Cartesian coordinates, and the corresponding time step takes $\delta t = 1$.

The nominal fluid density is set at $\rho = 1.0$, the translation velocity, V_t, and the cylinder diameter, D, are taken as the characteristic velocity and length, respectively. The motion of rotationally oscillating cylinder is prescribed by the following time-dependent angular velocity:

$$\omega(t) = \omega_0 \sin(2\pi f t) = A\frac{2V_t}{D}\sin\left(2\pi St\frac{V_t}{D}t\right) \tag{26}$$

where f and ω_0 are the frequency and base rotation rate, respectively. These two parameters can be normalized by introducing two non-dimensional parameters: Strouhal number, $St = \frac{fD}{V_t}$, and the normalized rotation rate, $A = \frac{\omega_0 D}{2V_t}$. This validation case employs $A = 2.0$, $Re = 100$, and $St = 0.163$ in accordance with the available references [32,33]. As illustrated in Fig. 2, the instantaneous vorticity field obtained using IB-LBM matches well with the results of Wu et al. [32] and Choi et al. [33]. The vortex shedding phenomenon can be clearly observed using the present method, and the patterns of the vortices released from the obstacle look overall the same, as shown in Fig. 2.

The validation can also be performed using the time-averaged drag coefficient, $\overline{C_d}$, and the maximum amplitude of the lift coefficient fluctuation, C_l', leading to a quantitative comparison against existing references [32,33] as depicted in Table 1. Here, $St = 0.4$

is taken since [32,33] examined this Strouhal number for evaluation of these two parameters; other parameters remain the same as aforementioned. Both $\overline{C_d}$ and C_l' obtained in this study are found comparable with the results reported in [32,33], as demonstrated in Table 1. The small differences may be attributed to the computational domain and meshing arrangement that were employed differently in the three simulation sets of this benchmark case. Through comparisons of the vorticity contour and aerodynamic parameters, the present IB-LBM framework exhibits its reliability for complex rotational flow simulations. Besides, the grid independency study corresponding to the IB-LBM framework was conducted previously [34], revealing that this integrated numerical approach has approximately the second order of accuracy, and the results can be considered as grid-independent when the grid resolution is finer than 1/40, i.e., the length of cylinder diameter should be uniformly divided into 40 or more equal portions when discretizing the computational domain. The present tornado study employs this numerical framework with a grid resolution of 1/50, and it is reasonable to believe the resulting simulation is reliable.

5. Numerical experiments

The stylized building configuration for test use in this study includes two identical cylinders of diameter D that are gapped by $3D$ and oriented in three manners facing the incoming translation of a tornadic wind: vertical, horizontal, and 45°-inclined. Assign $D = 20$ m and $V_t = 20$ m/s (towards the positive x-direction) for the tornado-construction interaction scenario under numerical investigation. If taking D as 1 unit of length, then, for all subsequent simulations, the computational domain occupies a $[-40,40] \times [-12.5,12.5]$ rectangular domain. Recall that a tornado passing over a building is interpreted in this study as a superposition of a "*pinned*" rotational airflow and a "*virtual translation*" of the building in the opposite direction of the tornado translation component, which is the re-tailored version of RCVM in order to render the outer velocity boundary condition time-independent. Using the re-tailored RCVM, the center of the counterclockwise rotational flow component is fixed at (0,0), and the building configuration center is initially placed at (35,0) with a constant translational speed towards the negative x-direction, which is opposite to the physical scenario where the tornado is translating to the positive x-direction.

For each orientation, the testing Reynolds number ranges from 1000 to 3500 through adjusting the fluid viscosity while locking the characteristic velocity, V_t, and length, D. At such moderate and higher Reynolds numbers, the MRT techniques have some difficulties associated with the formulation of viscosities, and a subgrid stress (SGS) model has to be appended to the IB-LBM framework to counteract those problems. Three loading coefficients, C_x, C_y, and C_m, which reflect the aerodynamic force components in the x- and y-directions, F_x, F_y, and the resulting moment, M, respectively, are defined as:

$$C_x = \frac{F_x}{0.5\rho V_t^2 D} \tag{27}$$

$$C_y = \frac{F_y}{0.5\rho V_t^2 D} \tag{28}$$

$$C_m = \frac{M}{0.5\rho V_t^2 (\pi D^2/4)} \tag{29}$$

These coefficients can serve to examine the wind loading on the cylinders. This study will evaluate the relation between Re and the aerodynamic force, i.e., wind loading, exerted on bi-cylinder configurations when different rotation intensities are present in the tornadoes, aiming to capture the critical rotation intensity beyond which the deviation in tornado characteristics arises. Remark that five mesh resolutions at 1/40, 1/50, 1/60, 1/80, and 1/100 were tested for the case with $Re = 3500$, which is the biggest Reynolds number investigated in the present study, confirming that the 1/50 grid resolution remains a compromising choice, echoing the conclusion from the aforementioned previously conducted grid independency study [34]. Thus, for all subsequent simulations, the computational domain is uniformly discretized such that the length of D (cylinder diameter) is equally divided into 50 "lattice units", which means one lattice unit, $\delta x = \delta y$, is equivalent to $\frac{20m}{50} = 0.4$ m in the present simulations. According to the conversion system described in [35], if taking the sonic speed of air approximately at 340 m/s, one time step used in LBM, δt, is equivalent to 6.79×10^{-4} s, and the translational speed, $V_t = 20$ m/s, represents 0.03396 lattice unit per time step in LBM.

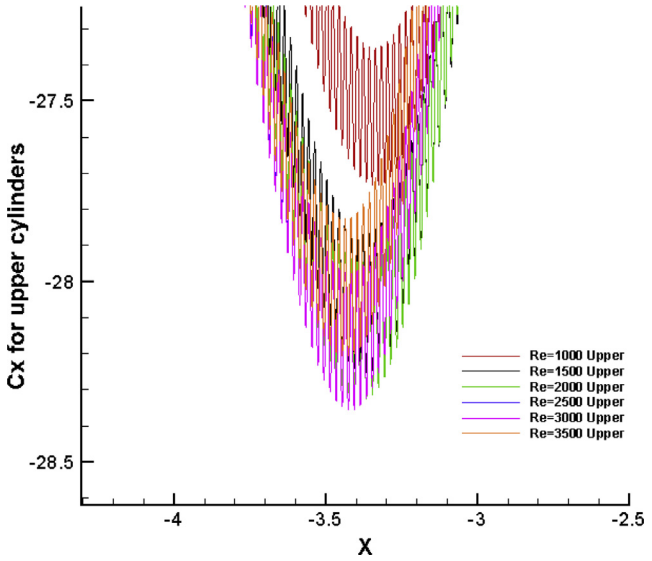

Fig. 8. C_x extreme points (for the upper cylinder) for vertically arranged bi-cylinders at $\beta = 2$, under different Re.

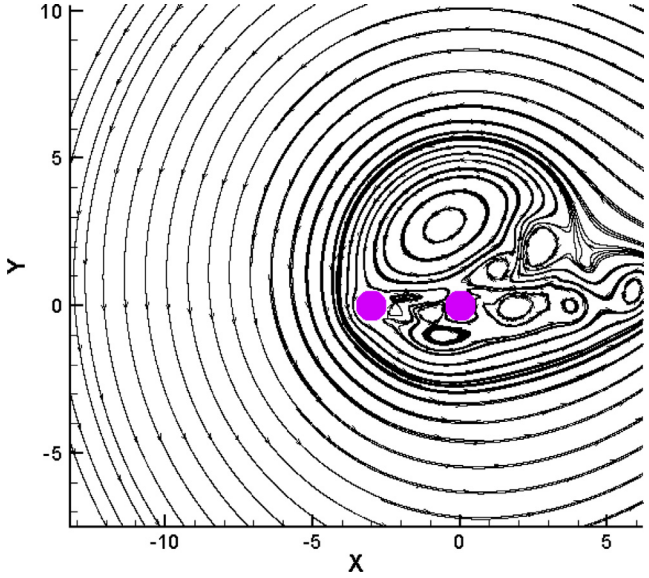

Fig. 9. Streamlines at "coinciding-center" time for horizontally arranged bi-cylinders, at $Re = 1000$ and $\beta = 1$.

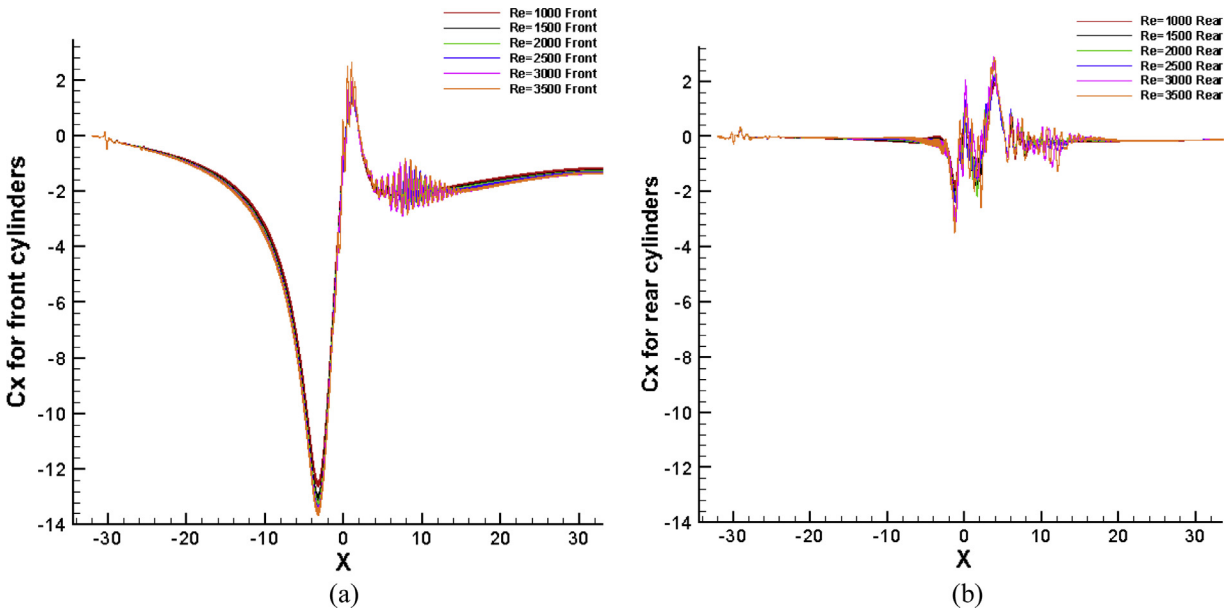

Fig. 10. C_x evolutions for horizontally arranged bi-cylinders at $\beta = 1$, under different *Re* (a) front cylinder; (b) rear cylinder.

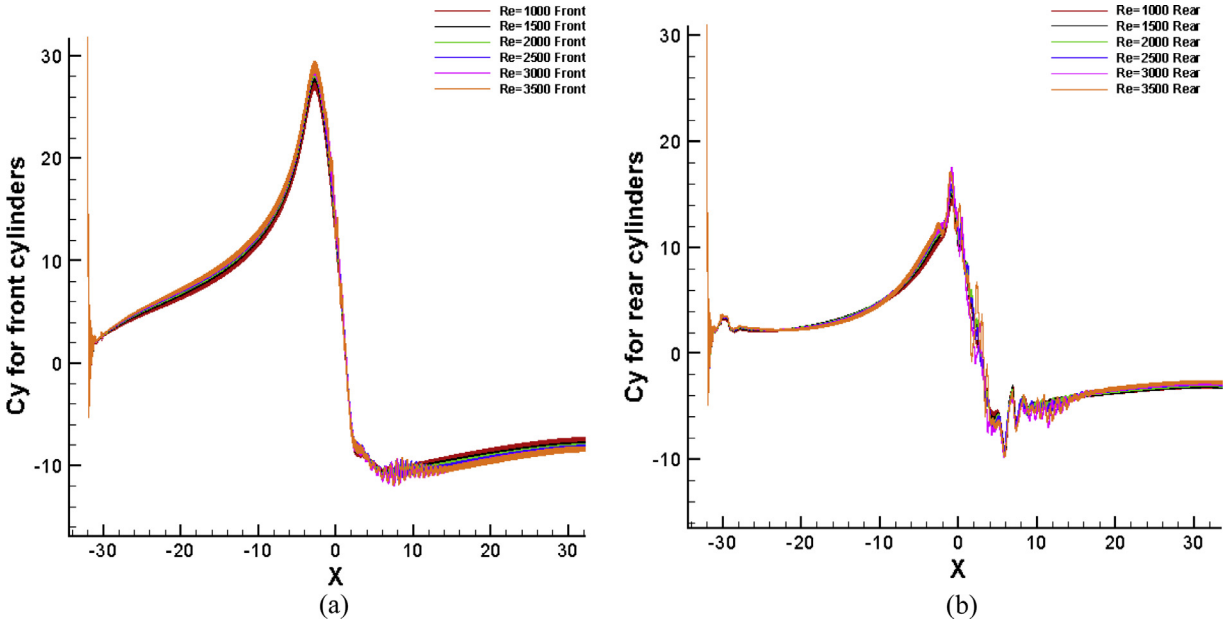

Fig. 11. C_y evolutions for horizontally arranged bi-cylinders at $\beta = 1$, under different *Re* (a) front cylinder; (b) rear cylinder.

Recall that, in Section 2.1, the *forced-vortex region* in RCVM is defined as a circle that spans from the tornado center up to the critical radius, r_c ($r_c = 3D$), at which the local tangential velocity component reaches its maximum value. This forced-vortex region is also referred to as "*tornado core zone*". For the sake of description convenience, particular attention will be paid to the flow behavior at three characteristic time points during the tornado-building interaction, namely, (1) the tornado core zone starts touching the building, i.e., $x_{building\_center} - x_{tornado\_center} = r_c$, which is referred to as "*core-in*" time; (2) the tornado and building centers are coinciding, i.e., $x_{building\_center} = x_{tornado\_center}$, which is referred to as "*coinciding-center*" time; and (3) the tornado core zone completely leaves the building, i.e., $x_{tornado\_center} - x_{building\_center} = r_c$, which is referred to as "*core-out*" time. Remark that the names of these three time points do not suggest the onset of such phenomena in their exact sense since, obviously, the interaction between the tornadic wind and building physically takes place when $x_{building\_center} - x_{tornado\_center} > r_c$. Between the "*core-in*" and "*core-out*" time points is the *primary* stage of the tornado-building interaction, whereas before and after the primary stage are respectively referred to as *pre-interaction* and *post-interaction* stages.

5.1. Vertically arranged bi-cylinders

First, two vertically arranged cylinders are tested. Under rotation intensity $\beta = 1.5$, the simulation results of the streamline pattern with $Re = 1000$ at the "*coinciding-center*" time, along with the C_x, C_y, and C_m evolutions at different testing Reynolds numbers are respectively plotted in Figs. 3–6. Note the horizontal coordinate, X,

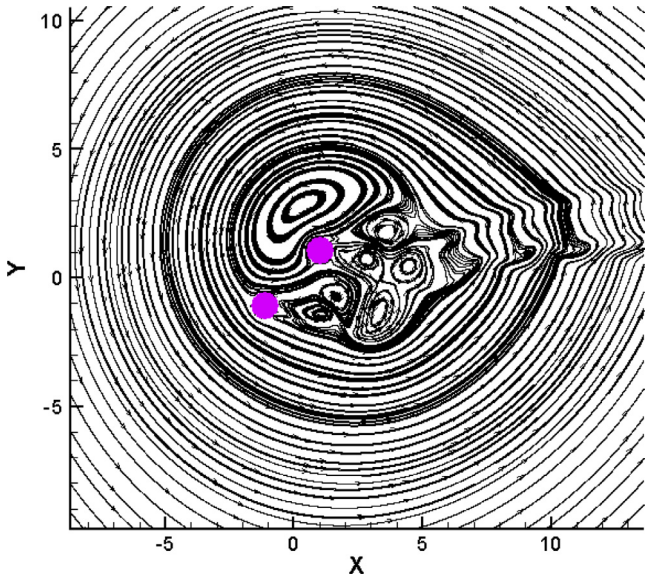

Fig. 12. Streamlines at "coinciding-center" time for inclined bi-cylinders, at $Re = 1000$ and $\beta = 1.375$.

in Figs. 4–6 is arranged such that, while X < 0, X = 0, and X > 0, the tornado center approaches the construction, coincides with the construction center in the nominal sense, and leaves the construction, respectively.

When the translating tornado center approaches the bi-cylinder construction, Fig. 3 demonstrates that the tornado core area is strongly disturbed with two series of eddies found in the wake region, suggesting the local dominance of the translational flow component upon recalling the renowned Karman vortex street phenomenon that arises in the case of a single cylinder facing a purely translational incoming flow with an elevated Reynolds number. On the other hand, due to the elapsing tornado-construction interaction, at the nominal "coinciding-center" time, Fig. 3 does not illustrate the tornado and construction centers are exactly coinciding; instead, a slight upward trend is clearly seen for the flow in the wake region, which is attributed to the counter-clockwise rotational flow component in this tornadic wind. All observed characteristics collectively reflect the translation and rotation superposition nature of this tornadic wind. Consequently, the loadings C_x, C_y, and C_m on the upper cylinder can be observed apparently higher than those on lower cylinder, as shown in Figs. 4–6; also, the loading coefficients in both directions can be regarded as related with Reynolds number at $\beta = 1.5$, since the extreme points of C_x, C_y, and C_m monotonically increase with the Reynolds number.

However, the monotonicity between loading coefficients and Reynolds number is not persistent at all rotation intensities in the tornado case. When a more intense rotational component is present, such as $\beta = 2$, the extreme point of C_x at the "*core-in*" time no longer monotonically goes up with the increase of Reynolds number, as detected in Fig. 7 and further confirmed by an enlarged view in Fig. 8. Remark that the magnitude of C_x reaches its maximum when *Re* is 3000 although the upper limit of *Re* is 3500 in this test series. This suggests that, in the tornado dynamics study, the rotation intensity serves as a crucial parameter in addition to the Reynolds number that remains conventionally determined using only the incoming translation velocity component as the characteristic velocity.

By more detailed tests about the rotation intensity still over the same range of Reynolds number (from 1000 to 3500), the "*critical rotation intensity*" can be sought that discontinues the monotonicity of the aerodynamic forces with the increase of *Re*. A simple and yet efficient way to perform this search is to use the Newton's bi-section strategy. That is, given the numerical results corresponding to $\beta = 1.5$ and $\beta = 2$, the critical rotation intensity is believed to arise in the interval [1.5,2.0]. Then, the new testing rotation intensity is set using:

$$\beta_{new} = \frac{1}{2}(\beta_{mono} + \beta_{non-mono}) \tag{30}$$

for checking the monotonicity in question. After the monotonicity is confirmed at $\beta = 1.75$, β_{mono} is substituted by 1.75 to set a further rotation intensity for test use. Employing this bi-section method, the critical rotation intensity is found to be located within the interval [1.78125,1.8125], where $\Delta\beta = 1/32$ can be referred to as "*critical interval*" if this interval length is considered acceptably small. In other words, when the rotation intensity falls onto the left side of the critical interval, the wind loadings can be viewed as relevant mainly to Reynolds number, and the loading extreme point rises

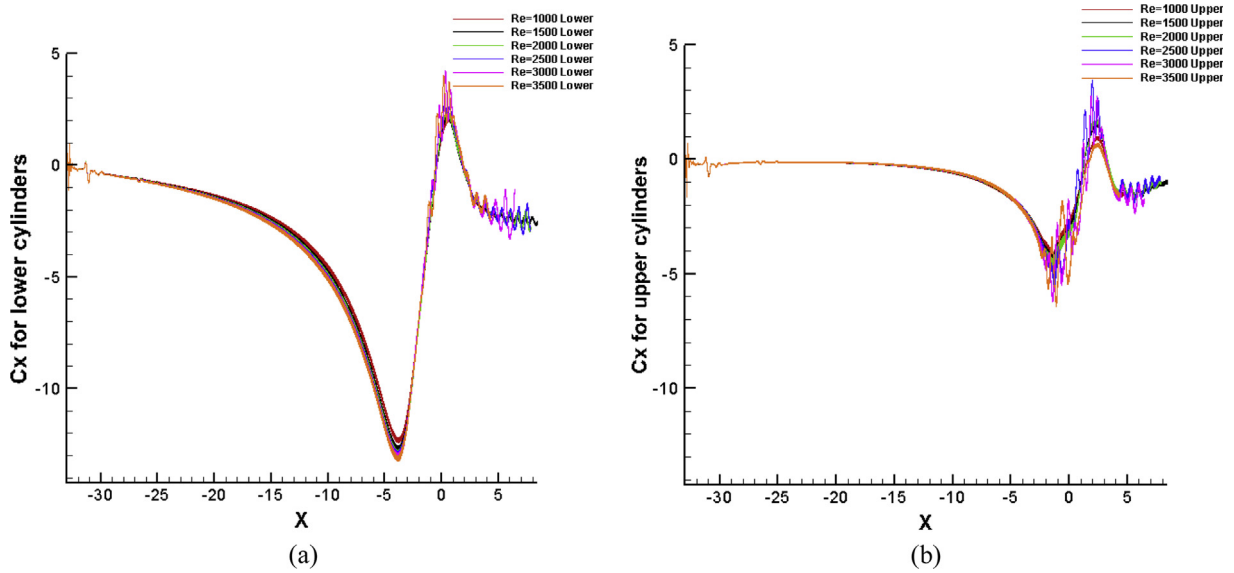

Fig. 13. C_x evolutions for inclined bi-cylinders at $\beta = 1.375$, under different *Re* (a) lower cylinder; (b) upper cylinder.

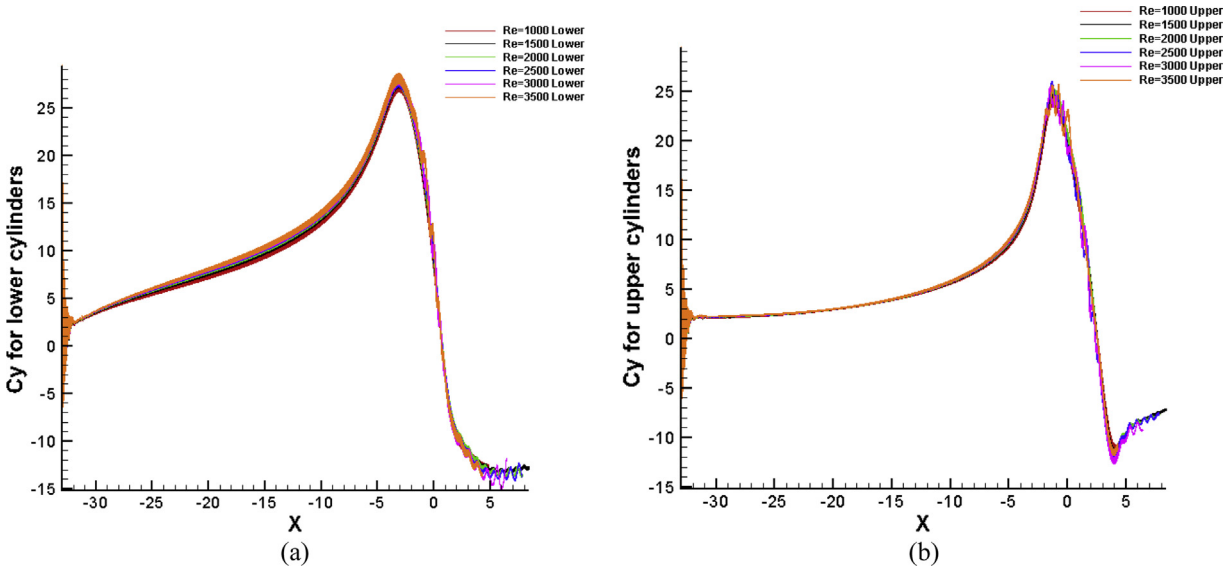

Fig. 14. C_y evolutions for inclined bi-cylinders at $\beta = 1.375$, under different *Re* (a) lower cylinder; (b) upper cylinder.

with the increase of *Re*; otherwise, there is no predictable relation between the loadings and *Re*. Hence, when the rotation intensity is above its critical value, the rotational component of a tornadic wind strongly affects the overall flow characteristics, and the translational velocity component based Reynolds number is no longer the sole dominant factor.

5.2. Horizontally arranged bi-cylinders

Now, the two cylinders are arranged horizontally. At *Re* = 1000 and $\beta = 1$, Fig. 9 illustrates the tornadic wind streamlines around the configuration corresponding to the "coinciding-center" time. Unlike in the precedent vertically arranged bi-cylinder case, only one Karman vortex street is evident in the wake; again, this vortex street still appears slightly upward due to the counter-clockwsie rotational component in the tornado.

The evolutions of force coefficients for both cylinders in Figs. 10 and 11 indicate that the trend of the loadings for the front cylinder overall matches with that for the upper one of the previous vertically arranged bi-cylinder; however, the force evolution for the rear cylinder here is observed to be in chaos. Facing the incoming hybrid flow, the front cylinder serves as a shelter to the rear cylinder, yielding a strong disturbance to the flow within the gap of the two cylinders and, hence, making it more difficult to predict the loading features for the rear cylinder. Despite the disordered loading evolution for the rear cylinder, the extreme loading measured on the front one at different Reynolds numbers still keep a monotonous trend as long as the rotation intensity is lower than its critical value. The critical intensity is found within the interval [1.09375, 1.125] (again, with $\Delta\beta = 1/32$ as critical interval) by using the Newton's bi-section method. Similar to the precedent case, when the rotation intensity β is higher than the critical value, Reynolds number is no longer the sole dominant factor; as seen in the relation between the maximum loading and *Re* for the front cylinder. As a matter of fact, both rotation intensity and *Re* co-play in such scenarios.

5.3. Inclined bi-cylinders

When two cylinders are placed to incline at 45° with respect to the horizontal to sustain a tornadic flow at *Re* = 1000 and β = 1.375, the indication of two series of shedding vortices, as shown in Fig. 12, is stronger than in the horizontally placed bi-cylinder case (see Fig. 9), but much weaker than in vertically placed bi-cylinder case (see Fig. 3). Similar to the case of horizontally arranged bi-cylinders, C_x on the front lower cylinder is observed to be higher than on the rear upper one, as seen in Figs. 13 and 14. Obviously, since physically the tornado core area reaches the front cylinder earlier than the rear one, the overall impulse provided by the aerodynamic forces would be bigger for the front cylinder. Again, of interest in this test case is to detect the critical rotation intensity by using the Newton's bi-section strategy. Here, the tests range for β from 0.5 up to 2, ending up with the critical value detected within [1.46875, 1.50] (with $\Delta\beta = 1/32$ as critical interval once more).

6. Concluding remarks

In this study, the conventional Rankine-Combined Vortex Model (RCVM) is revised to investigate the vortex-structure interaction through immersed boundary (IB) lattice Boltzmann method (LBM). The efficacy of the present IB-LBM framework with the customized RCVM is demonstrated through a validating case in which the vortex shedding pattern behind a rotationally oscillating cylinder is clearly seen and is corroborated with the references.

Numerous factors may affect the characteristics of a tornado-like wind. This study mainly concentrates on the relation between the rotation component and the acuteness of the tornado. The testing geometry is a configuration formed by two gapped cylinders of identical size. Three different orientations are investigated to simulate a tornado translating towards the bi-cylinder construction at attacking angles of 90° (Section 5.1), 0° (Section 5.2), and 45° (Section 5.3). Two terminologies are employed for evaluating the impact of the rotation intensity. The "*critical rotation intensity*" is defined such that the wind loadings monotonically rise with the increase of Reynolds number when the rotation intensity is lower than its critical value, and this monotonicity would disappear once the critical rotation intensity is reached or exceeded. To numerically detect this critical rotation intensity, the Newton's bi-section approach is proposed and, in practice, an acceptably small "*critical interval*" for accommodating the critical rotation intensity should be prescribed. Using $\Delta\beta = 1/32$ as critical interval for the three cases as aforementioned, the characteristic data are grouped in Table 2.

Table 2
Summarized results for three tested orientations.

Attack angle	Critical rotation intensity within	Largest C_x magnitude	Ratio of C_x extremes for the two cylinders
0°	[1.09375, 1.125]	13.6	6.6 (Fig. 10, for Re = 1000, β = 1)
45°	[1.46875, 1.5]	14.2	3.3 (Fig. 13, for Re = 1000, β = 1.375)
90°	[1.78125, 1.8125]	26.4	2.5 (Fig. 4, for Re = 1000, β = 1.5)

The second column of Table 2 reveals that, when the tornado translates at nil attack angle towards the bi-cylinder configuration, the critical rotation intensity is the smallest in the three orientation. At this orientation, a tornado with stronger rotational component might not severely damage the construction, which is justified by the third column (showing the largest C_x magnitude) of the table. However, in the horizontal arranged bi-cylinders, the fourth column (showing the ratio of the bigger C_x extreme for one cylinder to the smaller for the other cylinder) of the table warns that the front cylinder in the configuration would experience significantly larger wind loadings than the rear one, and the ratio appears larger than the other two cases. Not only may these findings help explain why within a building group swept by a tornado some buildings may survive while the others get violently demolished, but also lead to some insight and guidance for improving design of constructions towards better wind-resistant capabilities.

Another remark resulting from this study refers to the role of the rotation intensity in the tornado dynamics study. In tornado-like flows, the customary way of defining the Reynolds number with the translational velocity component as the characteristic velocity looks inequitable and equivocal, since the rotational velocity component plays an equally important role in determining the characteristics of tornadoes as well as imparting the annihilating potential to the tornado. At present, the critical rotation intensity is recommended as a complementary parameter for a more comprehensive study on the tornado dynamics.

The future work aims to extend the current two-dimensional RCVM-based IB-LBM framework to its three-dimensional version. This extension consists of two major aspects. First, the logarithmic law will be associated with the primitive RCVM to reflect the surface boundary layer growth with the altitude [14]. Second, the present 2-D IB-LBM framework needs to be enhanced to accommodate a 3-D construction. Given the reported success in 3-D IB-LBM simulations [36,37], it looks promising for the development of the present 2-D tornado simulation model towards its use for numerical investigation of more realistic tornado-building interaction scenarios in the 3-D context.

Acknowledgement

This study was fully financially funded by the Discovery Grant of the Natural Sciences and Engineering Research Council (NSERC) of Canada. The authors also wish to thank the High Performance Computing Virtual Laboratory (HPCVL) for providing the computational facilities in support of the computations reported here.

References

[1] Rotunno R. The fluid dynamics of tornadoes. Annu Rev Fluid Mech 2013;45(1):59–84.
[2] Ward NB. The exploration of certain features of tornado dynamics using a laboratory model. J Atmos Sci 1972;29:1194–204.
[3] Haan F, Sarkar P, Gallus WA. Design, construction and performance of a large tornado simulator for wind engineering applications. Eng Struct 2008;30(4):1146–59.
[4] Tari PH, Gurka R, Hangan H. Experimental investigation of tornado-like vortex dynamics with swirl ratio: the mean and turbulent flow fields. J Wind Eng Ind Aerodyn 2010;98(12):936–44.
[5] Hu H, Yang Z, Sarkar P, Haan F. Characterization of the wind loads and flow fields around a gable-roof building model in tornado-like winds. Exp Fluids 2011;51(3):835–51.
[6] Wilson T, Rotunno R. Numerical simulation of a laminar end- wall vortex and boundary layer. Phys Fluids 1986;29(12):3993–4005.
[7] Nolan DS, Farrell BF. The structure and dynamics of tornado-like vortices. J Atmos Sci 1999;56:2908–36.
[8] Lewellen WS, Lewellen DC, Sykes RI. Large-eddy simulation of a tornado's interaction with the surface. J Atmos Sci 1997;54(5):581–605.
[9] Lewellen DC, Lewellen WS. Near-surface intensification of tornado vortices. J Atmos Sci 2007;64(7):2176–94.
[10] Ishihara T, Oh S, Tokuyama Y. Numerical study on flow fields of tornado-like vortices using the LES turbulence model. J Wind Eng Ind Aerodyn 2011;99(4):239–48.
[11] Bienkiewicz B, Dudhia P. Physical modeling of tornado-like flow and tornado effects on building loading. Proceedings of seventh US national conference on wind engineering 1993:95–106.
[12] Selvam RP, Millett PC. Computer modeling of tornado forces on buildings. Wind Struct 2003;6(3):209–20.
[13] Selvam RP, Millett PC. Large eddy simulation of the tornado-structure interaction to determine structural loadings. Wind Struct 2005;8(1):49–60.
[14] Gorecki P, Selvam RP. Rankine combined vortex interaction with a rectangular prism. Int J Comput Fluid Dynam 2015;29(1):120–32.
[15] Smagorinsky J. General circulation experiments with the primitive equations: I. The basic experiment*. Mon Weather Rev 1963;91(3):99–164.
[16] Aidun CK, Clausen JR. Lattice-Boltzmann method for complex flows. Annu Rev Fluid Mech 2010;42:439–72.
[17] Ladd AJC, Verberg R. Lattice-Boltzmann simulations of particle-fluid suspensions. J Stat Phys 2001;104(5–6):1191–251.
[18] Zhang J. Lattice Boltzmann method for microfluidics: models and applications. Microfluid Nanofluid 2011;10(1):1–28.
[19] Peskin CS. Flow patterns around heart valves: a numerical method. J Comput Phys 1972;10:252–71.
[20] Peskin CS. The immersed boundary method. Acta Numerica 2002;11:479–517.
[21] Feng ZG, Michaelides EE. The immersed boundary–lattice Boltzmann method for solving fluid–particles interaction problems. J Comput Phys 2004;195:602–28.
[22] Feng ZG, Michaelides EE. Proteus: a direct forcing method in the simulations of particulate flows. J Comput Phys 2005;202:20–51.
[23] Wu J, Qiu YL, Shu C, et al. An adaptive immersed boundary-lattice Boltzmann method for simulating a flapping foil in ground effect. Comput Fluids 2015;106:171–84.
[24] Wu J, Liu C, Yang SC, et al. Influence of a flexible tail on the performance of a foil hovering near the ground: numerical investigation. Eur J Mech-B/Fluids 2015;52:85–96.
[25] Tian FB, Luo H, Zhu L, Liao JC, Lu XY. An efficient immersed boundary-lattice Boltzmann method for the hydrodynamic interaction of elastic filaments. J Comput Phys 2011;230(19):7266–83.
[26] Zhang H, Tan Y, Shu S, et al. Numerical investigation on the role of discrete element method in combined LBM–IBM–DEM modeling. Comput Fluids 2014;94:37–48.
[27] Huang R, Wu H. An immersed boundary-thermal lattice Boltzmann method for solid–liquid phase change. J Comput Phys 2014;277:305–19.
[28] Lallemand P, Luo LS. Theory of the lattice Boltzmann method: dispersion, dissipation, isotropy, Galilean invariance and stability. Phys Rev E 2000;61(6):6546–62.
[29] Guo ZL, Zheng CG, Shi BC. Discrete lattice effects on the forcing term in the lattice Boltzmann method. Phys Rev E 2002;65(4):046308.
[30] Yuan R, Zhong C, Zhang H. An immersed-boundary method based on the gas kinetic BGK scheme for incompressible viscous flow. J Comput Phys 2015;296:184–208.
[31] Goldstein D, Handler R, Sirovich L. Modeling a no-slip flow boundary with an external force field. J Comput Phys 1993;105:354–66.
[32] Wu J, Shu C, Zhang YH. Simulation of incompressible viscous flows around moving objects by a variant of immersed boundary-lattice Boltzmann method. Int J Numer Meth Heat Fluid Flow 2010;62(3):327–54.
[33] Choi S, Choi H, Kang S. Characteristics of flow over a rotationally oscillating cylinder at low Reynolds number. Phys Fluids 2002;14(8):2767–77.
[34] Guo X, Yao J, Zhong C, Cao J. A hybrid adaptive-gridding immersed-boundary lattice boltzmann method for viscous flow simulations. Appl Math Comput 2015;267:529–53.
[35] Succi S. Lattice Boltzmann equation for fluid dynamics and beyond. Oxford University Press; 2001.
[36] Zhu L, He G, Wang S, et al. An immersed boundary method based on the lattice Boltzmann approach in three dimensions, with application. Comput Math Appl 2011;61(12):3506–18.
[37] Wu J, Shu C. An improved immersed boundary-lattice Boltzmann method for simulating three-dimensional incompressible flows. J Comput Phys 2010;229(13):5022–42.